RSC Advances

PAPER

Cite this: *RSC Adv.*, 2016, **6**, 29996

Large and porous carbon sheets derived from water hyacinth for high-performance supercapacitors

Kai Wu,†[a] Biao Gao,†[a] Jianjun Su,[a] Xiang Peng,[b] Xuming Zhang,*[ab] Jijiang Fu,[a] Shunjin Peng[a] and Paul K. Chu*[b]

Received 27th November 2015
Accepted 23rd February 2016

DOI: 10.1039/c5ra25098f

www.rsc.org/advances

To elevate the properties of carbon based electrical double-layer capacitors (EDLCs), sheet-like carbon with high porosity is desirable due to enhanced electron transport efficiency and good electrolyte accessibility. In this paper, large porous carbon sheets are fabricated *via* an acid treatment, pyrolytic carbonization, and alkali activation of water hyacinth (WH) biomass. The WH-derived carbon sheets with a large uniform area have a large specific surface of 1308 $m^2\ g^{-1}$ and desirable pore volume of 0.84 $cm^3\ g^{-1}$, resulting from the template of the original thin cell walls and large intercellular space, which deliver a high specific capacitance of 273 F g^{-1} at a current density of 1 A g^{-1}, excellent capacity retention of 75% when the current density is increased from 1 to 50 A g^{-1}, and superior cyclic stability over 10 000 cycles in 6 M KOH. The specific capacitance of the assembled symmetric capacitor based on the large and porous carbon sheets reaches a remarkable 81.5 F g^{-1} and an energy density of 7.24 W h kg^{-1} can be achieved at a current density of 1 A g^{-1}. These outstanding electrochemical properties suggest that the WH-derived porous carbon sheets have commercial potential in high-performance supercapacitors and the simple and economical process utilizing the WH waste biomass is environmentally friendly.

1. Introduction

On the heels of the increasing production of greenhouse gases due to the burning of fossil fuels, alternative clean energy sources and high-performance energy storage systems are attracting much attention.[1,2] Electrochemical energy storage is promising in many applications such as portable electronics, hybrid electrical vehicles, and renewable energy storage.[3] With regard to green and economical mass production, the proper utilization of natural resources is a priority and materials derived from biomass have attracted increasing attention. In our previous work, rice husks[4] and bamboo leaves[5] were used as sustainable sources to produce ultrafine silicon (Si) nanoparticles *via* thermal decomposition. The nanoscale Si delivers a high performance for Li-ion battery anodes boasting a high reversible capacity and long cycle life time. However, the conversion yield of Si nanoparticles from organic precursors is quite low (5% by weight). Except for in high value adding Li-ion battery anode materials, carbon material obtained from waste biomass is an important product. However, it is challenging to prepare high-performance carbon-based materials from natural resources or industrial waste with high efficiency.

Nanostructured carbon materials such as activated carbon, graphene, carbon nanotubes, and carbon nanofibers are widely used in sensing, catalysis, and lithium ion batteries, as well as electrical double-layer capacitors (EDLCs) on account of their large surface area, excellent conductivity, and physical/chemical stability.[6–10] In particular, carbon-based EDLCs employing porous carbon produced from waste biomass have gained much attention due to their high power density, long cycles, considerable energy density, and environmental friendliness and they have many advantages over Li-ion batteries and traditional capacitors.[11–23] However, most of the materials have a finite rate performance and limited specific capacitance because of their granular structure resulting in low ion transport efficiency, a poor porous structure, and limited surface functions.[24]

Two-dimensional (2D) carbon materials are promising in next-generation supercapacitors and as important precursors for versatile three-dimensional (3D) porous carbon aerogels due to their high surface area, and ultralight weight as well as their good electrolyte accessibility as a result of a short ion transport and diffusion distance thus yielding enhanced rate performance and specific capacitance.[25–28] However, commercial processes for the fabrication of 2D carbon materials *via* exfoliating graphite oxide tend to be complex, expensive, and inefficient and the use of waste biomass to prepare 2D porous carbon is desirable. For instance, Wang *et al.* prepared interconnected carbon nanosheets from hemp and the materials had ultrafast electrochemical storage properties and good capacitance

[a]*State Key Laboratory of Refractories and Metallurgy, Wuhan University of Science and Technology, Wuhan 430081, P. R. China. E-mail: xumzhang@wust.edu.cn*

[b]*Department of Materials Science and Physics, City University of Hong Kong, Tat Chee Avenue, Kowloon, Hong Kong, China. E-mail: paul.chu@cityu.edu.hk*

† These two authors contributed equally to this work.

retention (>70% capacitance retained at a current density of 100 A g^{-1}).[25] Li *et al.* demonstrated the fabrication of N-doped porous carbon sheets *via* the one-step carbonization of a biomass precursor derived from eggplants and the material delivered a high rate performance due to the short ion diffusion paths and good retention (75% of the initial capacitance retained at a current density of 120 A g^{-1}).[27] However, the specific capacitance of these materials is still lower (about 100–150 F g^{-1}) than that of activated carbon. Fan *et al.* employed 2D microstructured gelatin as a carbon precursor and template to synthesize large porous carbon nanosheets with a high specific capacitance of 246 F g^{-1} and a capacitance retention of 82% at a current density of 100 A g^{-1}.[29] The selection of the bio-source precursors has been shown to be one of the most efficient strategies to prepare 2D porous carbon material for high performance supercapacitors.

In this paper, an environmentally friendly approach to synthesize large and porous carbon sheets from water hyacinths (WHs) is described. WHs, aquatic plants that grow quickly and can cause ecological problems, possess thin cell walls and large intercellular spaces and can be utilized in the adsorption of heavy ions from wastewater.[30] The unique microstructure of WHs bodes well for the preparation of large porous sheet-like carbon materials and the preparation procedures that are schematically illustrated in Fig. 1 are simple, economical, and environmentally friendly and can be readily scaled up for mass production. The large and porous carbon sheets have excellent electrochemical properties, such as high specific capacitance, and excellent rate capability, as well as a superior cyclic stability, making them potentially suitable for commercial energy applications.

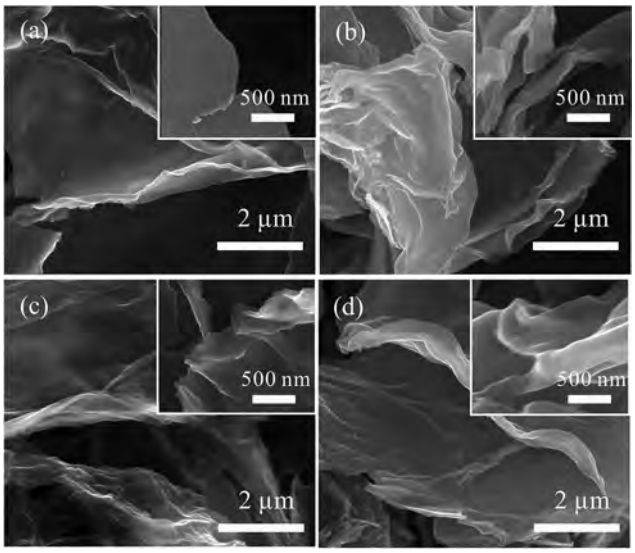

Fig. 2 (a) SEM images of the C-WH. SEM images of the AC-WH treated at (b) 700, (c) 800, and (d) 900 °C.

2. Experimental details

2.1 Material preparation

The WHs collected from a local lake (Wuhan, China) were cut into small pieces, washed with deionized (DI) water, and dried

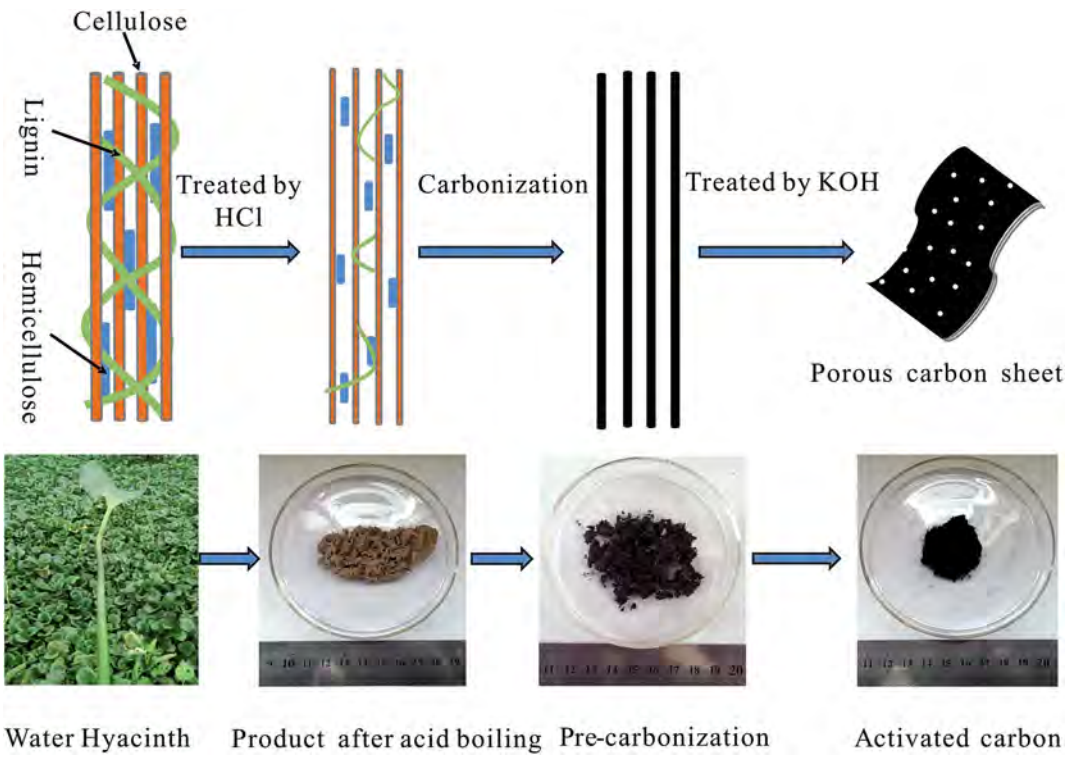

Fig. 1 Schematic illustration of the preparation process of AC-WH.

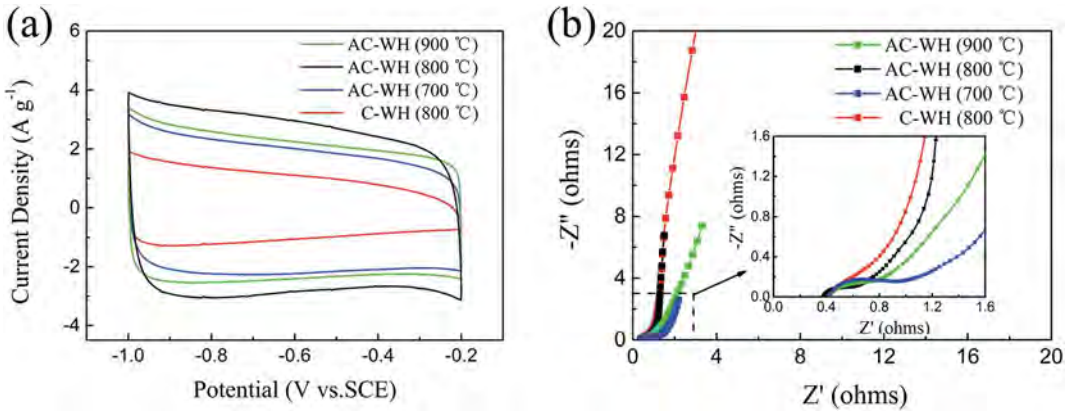

Fig. 3 (a) CV curves of C-WH and AC-WH prepared at 700, 800, and 900 °C at a scanning rate of 10 mV s^{-1} and (b) Nyquist plots of C-WH and AC-WH treated at 700, 800, and 900 °C. The measurements were performed in 6 M KOH at room temperature.

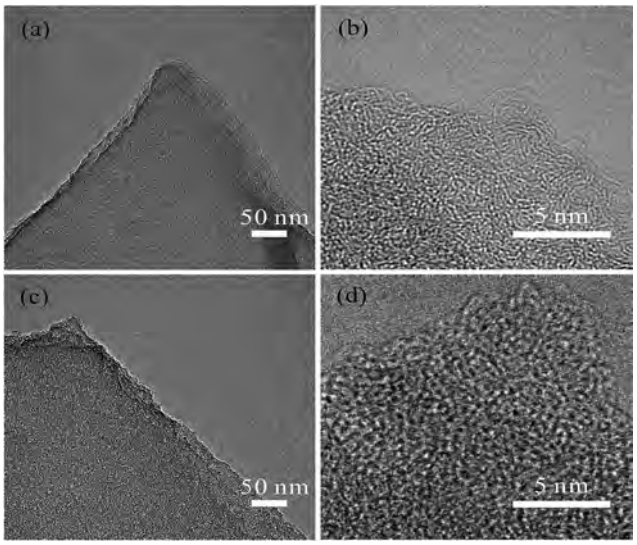

Fig. 4 Low- and high-magnification TEM images of the treated samples: (a) and (b) C-WH; (c) and (d) AC-WH (800 °C).

in an oven at 80 °C overnight. The dried WH was boiled in 0.25 M hydrochloric acid (HCl) for 12 h to remove metallic oxides and lignin and the product was washed with DI water several times and dried in a vacuum freeze-dryer for 24 h. The pre-carbonization was performed at 450 °C (5 °C min^{-1}) in a tubular furnace for 2 h under ambient N_2. Carbonized WH (C-WH) was obtained by annealing the pre-carbonized product at 800 °C for 2 h under N_2 flow and then the product was thoroughly ground for 1 hour as the comparison sample. The activated product was prepared *via* the following procedure: firstly, the pre-carbonized WH and KOH were mixed at a mass ratio of 1 : 1 and milled for 1 hour in a mortar, then the mixture was placed in a tubular furnace and calcined at different temperatures (700, 800 and 900 °C with heating rate of 5 °C min^{-1}) for 2 h under N_2 flow; afterwards, the activated pre-carbonized WH (AC-WH) was collected when the tubular furnace had cooled to room temperature naturally, and then rinsed with 1 M HCl and DI water several times, and dried in air.

2.2 Characterization

Field-emission scanning electron microscopy (FE-SEM, FEI Nova 400 Nano, Eindhoven, Netherlands), transmission electron microscopy (TEM, HRTEM, JEOL 2010, Tokyo, Japan), and X-ray photoelectron spectroscopy (XPS, ESCALB MK-II, VG Instruments, London, U.K.) were employed to investigate the morphology, microstructure, and composition of the samples. Raman scattering spectroscopy was conducted using a 514.5 nm argon laser as the excitation source on a Thermo Nicolet Almega XR Raman Microscope. The specific area was determined using the Brunauer–Emmett–Teller (BET) method using an automated chemisorption/physisorption surface area analyzer (Micromeritics ASAP 2020) at 77 K and the pore size distribution was determined using the Barrett–Joyner–Halenda (BJH) method. The specific area and pore size distribution were estimated using N_2 gas isothermal adsorption.

2.3 Electrode preparation and electrochemical measurements

The electrode materials composed of AC-WH, carbon black, and polytetrafluoroethylene (PTFE) were mixed at a weight ratio of 8 : 1 : 1 followed by grinding with several drops of ethanol for about 30 min. The mixture was painted onto nickel (Ni) foam at a known weight and dried at 100 °C in a vacuum oven overnight. The assembled Ni foam was pressed and weighed again before serving as the working electrode in a three-electrode system. To prepare the symmetric capacitor, the composite was rolled into a thin film with a diameter of 6 mm containing 1 to 2 mg of the active materials. A 2016 type coin cell was assembled with two identical electrode films, two current collectors, and a separator together with several drops of the 6 M KOH electrolyte. A membrane filter (MPF50AC purchased from Nippon Kodoshi plant, Japan) was used as the separator.

The electrochemical measurements were performed on an electrochemical workstation (CHI660D, Shanghai, China) with a three-electrode configuration at a potential range between −1.0 and −0.2 V in 6 M KOH at room temperature. The assembled Ni foam was the working electrode and a platinum

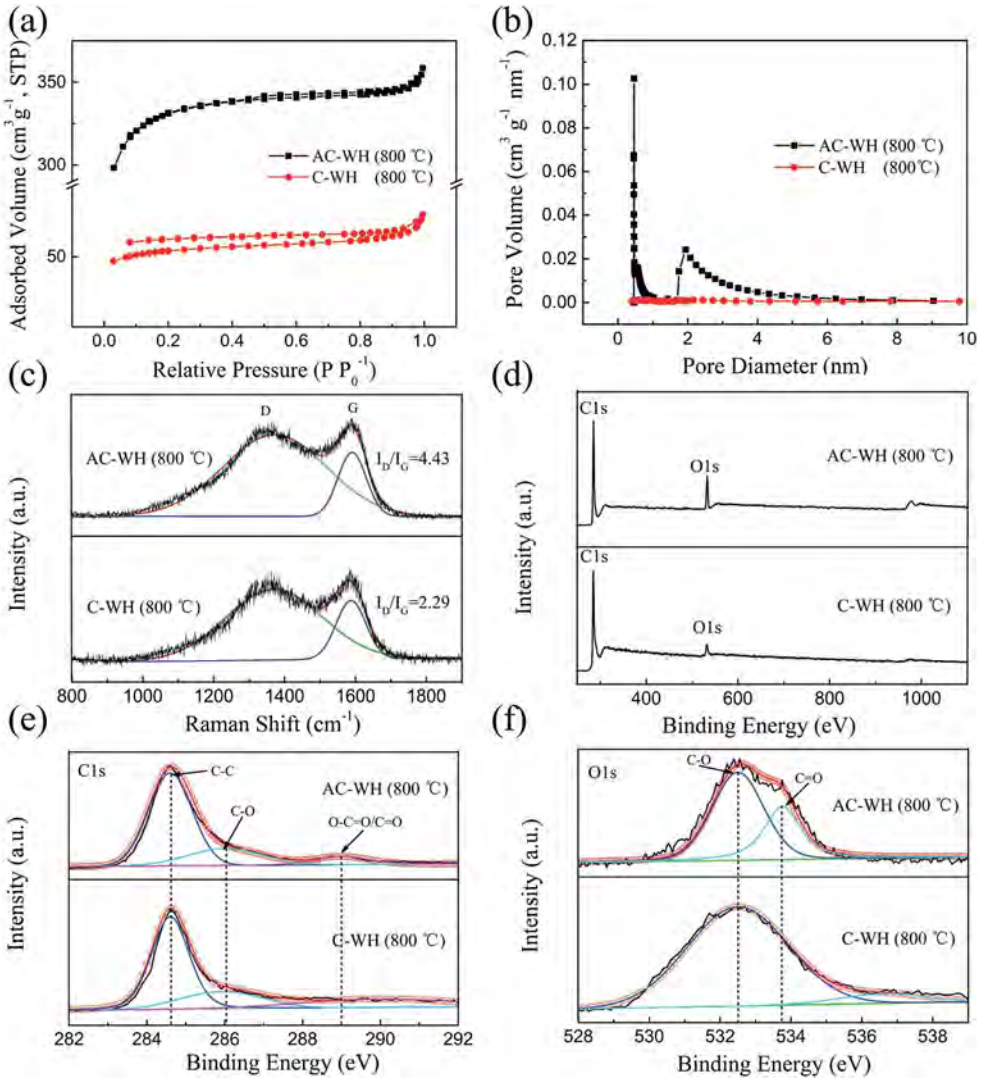

Fig. 5 (a) N_2 sorption isotherms and (b) corresponding pore size distribution; (c) Raman spectra; (d) full-scan XPS spectra; and high-resolution (e) C 1s and (f) O 1s spectra of C-WH and AC-WH (800 °C).

(Pt) foil and saturated calomel electrode (SCE) served as the counter electrode and reference electrode, respectively. Electrochemical impedance spectroscopy (EIS) was performed at the open-circuit potential with an AC perturbation voltage of 5 mV. Cyclic voltammetry (CV) and galvanostatic charge–discharge (GCD) measurements were performed to determine the electrochemical properties. In a symmetric two-electrode system, the coin cell was measured at a potential range from 0 to 0.8 V at room temperature. The capacitance (C (F)) and specific mass capacitance (C_m (F g^{-1})) in the three-electrode and symmetric two-electrode systems were measured and theoretically calculated using the following equations:

In the three-electrode system:

$$C_3 = \frac{I\Delta t}{\Delta V} \quad (1)$$

$$C_{3m} = \frac{C_3}{m} = \frac{I\Delta t}{m\Delta V} \quad (2)$$

In the ideally symmetric two-electrode system:

$$\frac{1}{C_2} = \frac{1}{C_3} + \frac{1}{C_3} = \frac{2}{C_3} \quad (3)$$

$$C_{2m} = \frac{C_2}{2m} = \frac{C_3}{4m} = \frac{C_{3m}}{4} \quad (4)$$

where I (A) is the constant discharge current, Δt (s) is the discharge time, ΔV (V) is the discharging potential range, and m (g) is the mass of the active materials on the single electrode.

3. Results and discussion

The chemical activation of carbon materials in the activating reagent KOH is a well-known method because of its lower activation temperature, and higher yields as well as it producing a well-defined micropore size distribution and high specific surface area.[31] Fig. 1 illustrates the process of carbonization and activation of WH. The color changes from green to dark yellow

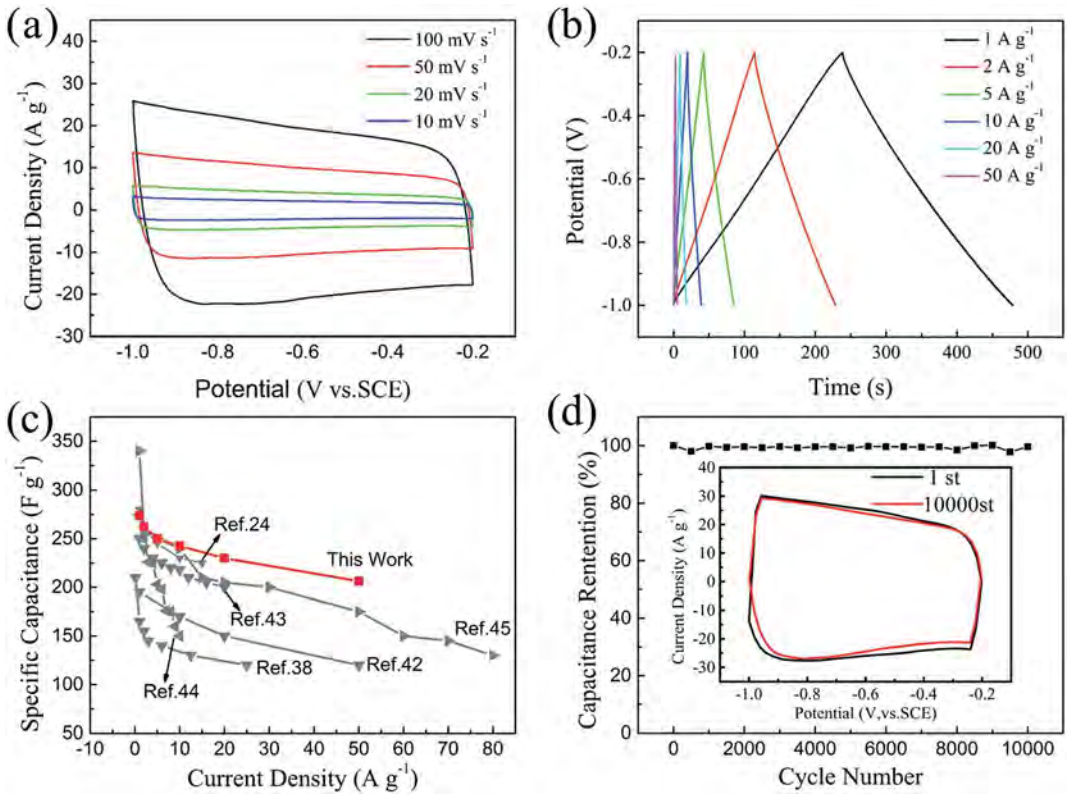

Fig. 6 (a) CV and (b) GCD curves of AC-WH (800 °C); (c) corresponding rate performance compared with the reference work; and (d) cycling life time of the AC-WH (800 °C) measured on the three-electrode system.

and then turns to black in the different steps. Fig. 2a displays an SEM image of the C-WH and a sheet-like product with a large uniform surface is observed. After activation in KOH at different temperatures, the morphology of the products changes slightly. Fig. 2b–d depict typical SEM images of C-WH activated at 700, 800, and 900 °C, respectively. Notably, the original sheet-like shape of the carbon precursors was well maintained, but there are many wrinkles on the surface of the microsheets due to the detachment of cellulose into individual microsheets during activation in KOH at 800 °C and above. The activation mechanism of carbon in KOH is complex and has not been well understood. Generally, the prominent reaction could start with a reaction as follows: $6KOH + 2C \rightarrow 2K + 3H_2 + 2K_2CO_3$. At a high activation temperature, the evolution of H_2, CO and CO_2 occurred *via* redox reactions between various potassium compounds and carbon.[31] The consumed carbon always generates micropores and small mesopores in the framework of various structured carbon materials.

The electrochemical properties of C-WH and AC-WH treated at 700, 800, and 900 °C were investigated in 6 M KOH at room temperature using a three-electrode configuration in the potential range between −1.0 and −0.2 V (*vs.* SCE). Fig. 3a presents the CV curves of C-WH and AC-WH obtained at a scanning rate of 10 mV s^{-1}. AC-WH shows nearly rectangular and symmetrical CV curves indicating excellent electric double layer capacitive performance. The area enclosed by the CV curve of AC-WH treated at 800 °C is much larger than that of pristine C-WH and other activated samples (treated at 700 and 900 °C). The specific capacitances of C-WH and AC-WH treated at 700, 800, and 900 °C are calculated to be 108, 218, 273, and 244 F g^{-1}, respectively. After carbonization and activation, EIS was performed and the results (shown in Fig. 3b) indicate that the charge-transfer resistance of AC-WH is 0.2 Ω which is smaller than that of C-WH (0.5 Ω).

The microstructure of the carbonized samples before and after KOH activation at 800 °C is characterized using TEM. As shown in Fig. 4a and b, C-WH has a multi-layered graphitic structure and the high-magnification TEM images reveal fringes in the carbonized microsheets indicating the onset of graphitization in the carbonization process. However, after activation in KOH, the order of the graphite layer fringes disappears and a disordered microstructure emerges throughout the microsheet due to etching using KOH (Fig. 4c and d).

The N_2 adsorption isotherm acquired at 77 K is employed to determine the pore distribution in the microsheet before and after KOH activation at 800 °C. Fig. 5a shows the specific surface area of C-WH and AC-WH. The specific surface area increases after activation from 171.5 m^2 g^{-1} on the original C-WH to 1308 m^2 g^{-1} on AC-WH and the pore volume changes from 0.1 to 0.84 cm^3 g^{-1}, correspondingly. Fig. 5b shows that AC-WH has both nanopores (0.4–0.7 nm) and mesopores (1.7–3 nm). The energy storage process in EDLCs occurs primarily on the exposed surface of the materials and a nanoporous structure typically yields limited enhancement pertaining to the electric double-

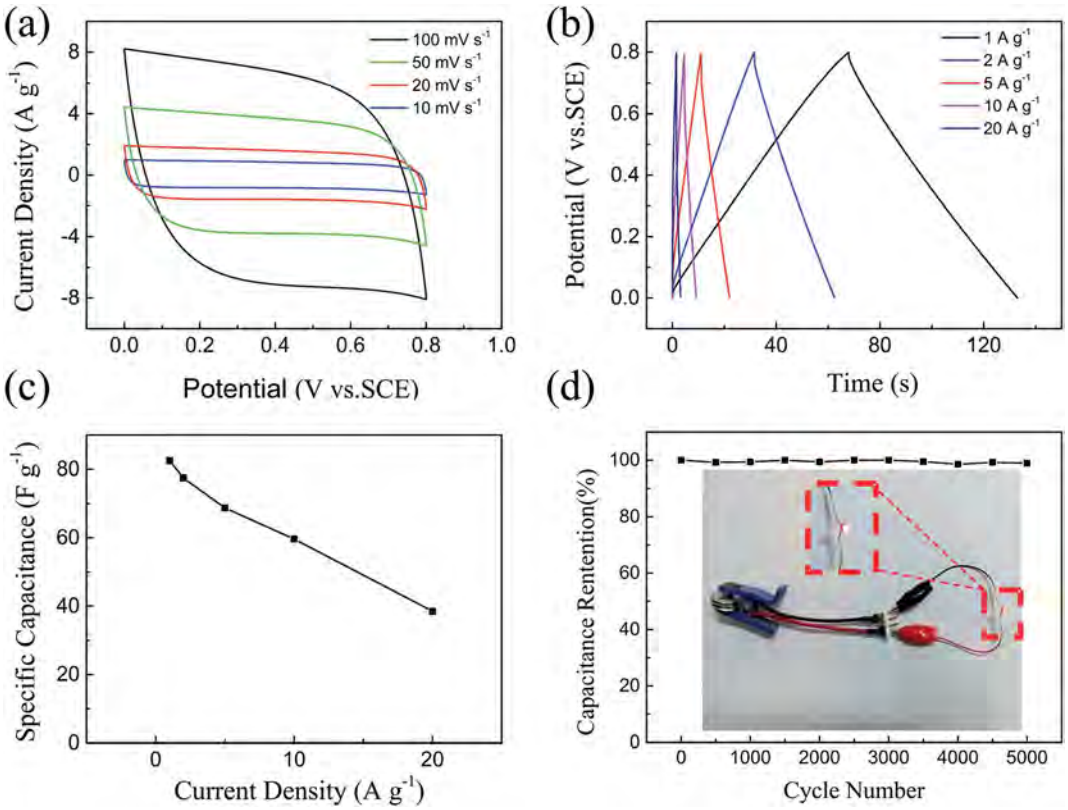

Fig. 7 (a) CV and (b) GCD curves of the symmetric capacitor based on AC-WH (800 °C); (c) rate performance of the symmetric capacitor; and (d) cycling performance of the symmetric capacitor measured in a two-electrode system.

layer capacitance due to limited electrolyte diffusion through the small pores.[32] In this respect, the presence of larger pores in AC-WH may improve electrolyte transport in the EDLCs.

The surface structure of C-WH and AC-WH is further studied *via* Raman scattering using a 514.5 nm Ar ion laser. As shown in Fig. 5c, both the carbonized and activated samples exhibit a broad disorder-induced D-band (~1330 cm^{-1}) and in-plane vibrational G-band (~1590 cm^{-1}). The D-band is due to the breathing mode of *k*-point phonons of A_{1g} symmetry which corresponds to defects and disorder-induced structures, whereas the G band arises from the vibration of sp^2 carbon atoms in a two-dimensional hexagonal lattice in the graphitic layers. The intensity ratio of the D band to the G band (I_D/I_G) indicates the degree of graphitic ordering.[33] Here, AC-WH shows a larger I_D/I_G ratio (4.43) than C-WH (2.29) indicating a more disordered structure consistent with the TEM observation.

The chemical composition and the oxidation states of C-WH before and after activation at 800 °C are determined using XPS. Fig. 5d displays the survey scan spectra from 200–1100 eV showing two representative peaks at 284.6 and 532.5 eV corresponding to C 1s and O 1s,[34] respectively and no metallic elements before and after activation. The atom content of C and O in C-WH was changed from 91.3% and 8.8% to 87.8% and 12.2% after activation at 800 °C. The deconvoluted C 1s peak of C-WH shows the presence of C–C bonds in the graphite domains (284.6 eV) and C–O groups (285.7–286.1 eV).[35,36] The high-resolution C 1s peak observed from AC-WH can be fitted with three peaks, verifying the presence of complex carbonyl groups (C=O/O–C=O: 288.4–289.1 eV)[23,37] and indicating the introduction of oxygen-containing functional groups by alkali activation, as shown in Fig. 5e. The enhanced intensity of the carboxyl and/or ester peak at 289 eV indicates that etching of C-WH by KOH leads to a lower degree of graphitic ordering and the formation of oxygen-containing functional groups which favor pseudocapacitance.[22,38] The high-resolution O 1s spectrum of C-WH shows one main peak at 532.5 eV corresponding to a C–O bond[39] and with regard to AC-WH, there are two fitted peaks in the O 1s spectrum at 532.5 and 533.8 eV representing C–O and C=O bonds, respectively (Fig. 5f).[40] XPS shows the existence of oxygen-containing functional groups after activation and they can increase the faradic reactions, improve the wettability of the carbon materials, and enhance the capacity in an aqueous electrolyte.

Chemical activation is a useful approach to create additional micropores and larger surface areas as well as a higher content of oxygen-containing groups, thus favoring electrolyte contact and diffusion and enhancing electrochemical performance.[41] To evaluate the electrochemical performance of AC-WH (800 °C), CV and GCD measurements were conducted in 6 M KOH using a three-electrode system. Fig. 6a displays the typical CV curves at scanning rates from 10 to 100 mV s^{-1}. All of the curves show a quasi-rectangular shape, indicating the fast charging/discharging of an ideal EDLC. Fig. 6b presents the GCD

curves of AC-WH in a potential range between −1 and −0.2 V (*vs.* SCE) at current densities from 1 to 50 A g^{-1}. The GCD curves show an almost symmetrical shape with slight distortion indicative of a good capacitive behavior of the EDLCs coupling with a weak pseudocapacitance reaction. The specific capacitance can reach 273 F g^{-1} at a small current density of 1 A g^{-1} and is retained at 206 F g^{-1} at a high current density of 50 A g^{-1}. This is about 75% of the initial capacitance, implying that WH derived carbon materials deliver excellent capacitive performances. The relationship between the specific capacitance calculated from the discharging time and discharge current densities is shown in Fig. 6c. According to our experimental results, the electrochemical properties of AC-WH (800 °C) are better than those of activated carbon derived from other biomass materials such as pomelo peels,[24] fungi,[42] peanut shells,[38] chicken eggshell membranes,[43] sunflower seed shells,[44] and human hair.[45] The cycling performance of AC-WH is also evaluated using CV curves, which are shown in Fig. 6d. The specific capacitance retains 99% of the initial capacitance after 10 000 consecutive CV cycles demonstrating excellent cycling stability. The capacitive performance can be attributed to the large sheet-like microstructure containing micropores and mesopores providing a short ion/electron diffusion distance and large surface area.

In order to demonstrate the feasibility of AC-WH in a supercapacitor, a symmetric capacitor is assembled and tested in the potential range between 0 and 0.8 V. As shown in Fig. 7a and b, the CV curves retain the rectangular shape as the scanning rate is varied from 10 to 100 mV s^{-1} and the GCD plot results show good symmetry when the current density is increased from 1 to 20 A g^{-1}. Both indicate excellent capacitive reversibility. The specific capacitance of the symmetric capacitor reaches 81.5 F g^{-1} and an energy density of 7.24 W h kg^{-1} at a current density of 1 A g^{-1} is accomplished. Because of the serial connection of the two electrodes in a symmetric capacitor, the specific mass capacitance measured in the device is about one fourth of the capacitance obtained in the three-electrode system. The device retains 47% of the initial capacitance (38.5 F g^{-1}) when the current density is increased 20 times (Fig. 7c). In addition, the symmetric capacitor has an excellent long-term cycling life. After 5000 CV cycles at a scanning rate of 100 mV s^{-1}, 99% of the initial capacitance is retained (Fig. 7d) and a red light-emitting diode with a threshold voltage of 1.8 V can be driven by three devices in series.

4. Conclusion

Large porous carbon sheets are produced *via* an acid treatment, pyrolytic carbonization, and KOH activation of water hyacinth (WH) biomass. After carbonization and activation, large carbon sheets composed of micropore and mesopore structures are obtained. The materials have a large specific area and deliver a desirable capacitance and rate performance in EDLCs. In particular, in a three-electrode system, the specific capacitance of the carbon sheets treated at 800 °C is as high as 273 F g^{-1} at a current density of 1 A g^{-1} and 206 F g^{-1} (75% of initial capacitance) is retained when the current density is increased to 50 A g^{-1}. They also have good cycling stability and 99% of the capacitance is retained after 10 000 successive CV cycles. The symmetric capacitor prepared with AC-WH shows a large specific capacitance of 81.5 F g^{-1} at a current density of 1 A g^{-1}. Our results reveal a simple and environmentally friendly strategy to produce large carbon sheets with the desirable specific area and microstructure suitable for advanced energy storage devices.

Acknowledgements

This work was financially supported by Natural Science Foundation of China (51504171, 51572100, 31500783), Project of Hubei Provincial Education Office (B2015346), Outstanding Young and Middle-aged Scientific Innovation Team of Colleges and Universities of Hubei Province (T201402), Applied Basic Research Program of Wuhan City (2013011801010598), Project of Natural Science Foundation of Hubei Province (2015CFA116), City University of Hong Kong Applied Research Grant (ARG) No. 9667104, and Guangdong – Hong Kong Technology Cooperation Funding Scheme (TCFS) No. GHP/015/12SZ.

References

1 P. Simon and Y. Gogotsi, *Nat. Mater.*, 2008, **7**, 845–854.
2 S. F. Tie and C. W. Tan, *Renewable Sustainable Energy Rev.*, 2013, **20**, 82–102.
3 G. P. Wang, L. Zhang and J. J. Zhang, *Chem. Soc. Rev.*, 2012, **41**, 797–828.
4 N. Liu, K. F. Huo, M. T. McDowell, J. Zhao and Y. Cui, *Sci. Rep.*, 2013, **3**, 1919.
5 L. Wang, B. Gao, C. J. Peng, X. Peng, J. J. Fu, P. K. Chu and K. F. Huo, *Nanoscale*, 2015, **7**, 13840–13847.
6 F. Rodríguez-reinoso, *Carbon*, 1998, **36**, 159–175.
7 L. S. Hu, K. F. Huo, R. S. Chen, X. M. Zhang, J. J. Fu and P. K. Chu, *Chem. Commun.*, 2010, **46**, 6828–6830.
8 B. Z. Fang, A. Bonakdarpour, M. S. Kim, J. H. Kim, D. P. Wilkinson and J. S. Yu, *Microporous Mesoporous Mater.*, 2013, **182**, 1–7.
9 J. Li, Y. J. Lu, Q. Ye, M. Cinke, J. Han and M. Meyyappan, *Nano Lett.*, 2003, **3**, 929–933.
10 N. Li, Z. P. Chen, W. C. Ren, F. Li and H. M. Cheng, *Proc. Natl. Acad. Sci. U. S. A.*, 2012, **109**, 17360–17365.
11 P. Kalyani and A. Anitha, *Int. J. Hydrogen Energy*, 2013, **38**, 4034–4045.
12 Z. Q. Niu, H. B. Dong, B. W. Zhu, J. Z. Li, H. H. Hng, W. Y. Zhou, X. D. Chen and S. S. Xie, *Adv. Mater.*, 2013, **25**, 1058–1064.
13 M. Sevilla and R. Mokaya, *Energy Environ. Sci.*, 2014, **7**, 1250–1280.
14 P. H. Yang, Y. Ding, Z. Y. Lin, Z. W. Chen, Y. Z. Li, P. F. Qiang, M. Ebrahimi, W. J. Mai, C. P. Wong and Z. L. Wang, *Nano Lett.*, 2014, **14**, 731–736.
15 X. J. He, P. H. Ling, J. S. Qiu, M. X. Yu, X. Y. Zhang, C. Yu and M. D. Zheng, *J. Power Sources*, 2013, **240**, 109–113.
16 S. Kumagai, M. Sato and D. Tashima, *Electrochim. Acta*, 2013, **114**, 617–626.

17 C. C. Huang, A. M. Puziy, T. Sun, O. I. Poddubnaya, F. Suárez-García, J. M. Tascón and D. Hulicova-Jurcakova, *Electrochim. Acta*, 2014, **137**, 219–227.
18 Y. X. Wang, Y. F. Song, Y. Wang, X. Chen, Y. Y. Xia and Z. Z. Shao, *J. Mater. Chem. A*, 2015, **3**, 773–781.
19 H. P. Li, B. Wang, X. Y. He, J. Xiao, H. S. Zhang, Q. Liu, J. Y. Liu, J. Wang, L. H. Liu and P. Wang, *J. Mater. Chem. A*, 2015, **3**, 9754–9762.
20 J. L. Chang, Z. Y. Gao, X. R. Wang, D. P. Wu, F. Xu, X. Wang, Y. M. Guo and K. Jiang, *Electrochim. Acta*, 2015, **157**, 290–298.
21 J. F. Li, S. W. Ma, L. Y. Cheng and Q. S. Wu, *Mater. Lett.*, 2015, **139**, 429–432.
22 Q. H. Liang, L. Ye, Z. H. Huang, Q. Xu, Y. Bai, F. Y. Kang and Q. H. Yang, *Nanoscale*, 2014, **6**, 13831–13837.
23 X. Wang, Z. Y. Gao, J. L. Chang, D. P. Wu, X. R. Wang, F. Xu, Y. M. Guo and K. Jiang, *RSC Adv.*, 2015, **5**, 15969–15976.
24 A. B. Fuertes and M. Sevilla, *ACS Appl. Mater. Interfaces*, 2015, **7**, 4344–4353.
25 H. L. Wang, Z. W. Xu, A. Kohandehghan, Z. Li, K. Cui, X. H. Tan, T. J. Stephenson, C. K. King'ondu, C. M. Holt and B. C. Olsen, *ACS Nano*, 2013, **7**, 5131–5141.
26 D. W. Wang, F. Li, M. Liu, G. Q. Lu and H. M. Cheng, *J. Phys. Chem. C*, 2008, **112**, 9950–9955.
27 Z. J. Li, W. Lv, C. Zhang, B. H. Li, F. Y. Kang and Q. H. Yang, *Carbon*, 2015, **92**, 11–14.
28 Y. Q. Qian, I. M. Ismail and A. Stein, *Carbon*, 2014, **68**, 221–231.
29 X. M. Fan, C. Yu, J. Yang, Z. Ling, C. Hu, M. D. Zhang and J. S. Qiu, *Adv. Energy Mater.*, 2015, **5**, 1401761.
30 K. Chunkao, C. Nimpee and K. Duangmal, *Ecol. Eng.*, 2012, **39**, 40–52.
31 J. C. Wang and S. Kaskel, *J. Mater. Chem.*, 2012, **22**, 23710–23725.
32 J. K. Ou, Y. Z. Zhang, L. Chen, Q. Zhao, Y. Meng, Y. Guo and D. Xiao, *J. Mater. Chem. A*, 2015, **3**, 6534–6541.
33 M. Wahid, D. Puthusseri, D. Phase and S. Ogale, *Energy Fuels*, 2014, **28**, 4233–4240.
34 Y. J. Li, N. Yu, P. Yan, Y. G. Li, X. M. Zhou, S. L. Chen, G. L. Wang, T. Wei and Z. J. Fan, *J. Power Sources*, 2015, **300**, 309–317.
35 C. L. Long, L. L. Jiang, X. L. Wu, Y. T. Jiang, D. R. Yang, C. K. Wang, T. Wei and Z. J. Fan, *Carbon*, 2015, **93**, 412–420.
36 G. Rasines, P. Lavela, C. Macías, M. Zafra, J. Tirado and C. Ania, *J. Electroanal. Chem.*, 2015, **741**, 42–50.
37 J. Yin, D. Y. Zhang, J. Q. Zhao, X. L. Wang, H. Zhu and C. Y. Wang, *Electrochim. Acta*, 2014, **136**, 504–512.
38 J. Ding, H. L. Wang, Z. Li, K. Cui, D. Karpuzov, X. H. Tan, A. Kohandehghan and D. Mitlin, *Energy Environ. Sci.*, 2015, **8**, 941–955.
39 J. Y. Qu, C. Geng, S. Y. Lv, G. H. Shao, S. Y. Ma and M. B. Wu, *Electrochim. Acta*, 2015, **176**, 982–988.
40 X. M. Fan, C. Yu, Z. Ling, J. Yang and J. S. Qiu, *ACS Appl. Mater. Interfaces*, 2013, **5**, 2104–2110.
41 V. Barranco, M. A. Lillo-Rodenas, A. Linares-Solano, A. Oya, F. Pico, J. Ibañez, F. Agullo-Rueda, J. M. Amarilla and J. M. Rojo, *J. Phys. Chem. C*, 2010, **114**, 10302–10307.
42 H. Zhu, X. L. Wang, F. Yang and X. R. Yang, *Adv. Mater.*, 2011, **23**, 2745–2748.
43 Z. Li, L. Zhang, B. S. Amirkhiz, X. H. Tan, Z. W. Xu, H. L. Wang, B. C. Olsen, C. Holt and D. Mitlin, *Adv. Energy Mater.*, 2012, **2**, 431–437.
44 X. Li, W. Xing, S. P. Zhuo, J. Zhou, F. Li, S. Z. Qiao and G. Q. Lu, *Bioresour. Technol.*, 2011, **102**, 1118–1123.
45 W. J. Qian, F. X. Sun, Y. H. Xu, L. H. Qiu, C. H. Liu, S. D. Wang and F. Yan, *Energy Environ. Sci.*, 2014, **7**, 379–386.